GEOPHYSICS, VOL. 68, NO. 6 (NOVEMBER-DECEMBER 2003); P. 1835–1846, 6 FIGS., 2 TABLES.
10.1190/1.1635036

Determination of thermal properties and formation temperature from borehole thermal recovery data

Tien-Chang Lee*, A. D. Duchkov‡, and S. G. Morozov ‡

ABSTRACT

Thermal recovery in boreholes cooled by circulation of drilling mud has been modeled for estimating formation temperature and thermal conductivity. Coupled with a finite-element simulation of heat conduction, inverse modeling for the desired parameters starts with a genetic algorithm that feeds initial estimates of model parameters to an iterative quasi-linear inversion scheme. In addition to using the rms misfit between the computed and observed borehole temperatures, the results are assessed by comparing or constraining the model formation temperature with a value obtained conventionally from an asymptotic temperature–time relation for a steady line source. The model conductivity is further evaluated for equality with a conductivity value, which is estimated through simulation of heat exchange between the formation and circulating mud. Test results on synthetic data and two sets of highly noisy borehole data from Lake Baikal in Russia indicate that the two equality criteria in temperature and conductivity are achievable. Multiple runs of GA-IM are used to find mean parameter values and their uncertainties. The resultant model conductivity values are consistent with those measured in cores with a needle-probe method.

INTRODUCTION

Drilling and mud circulation disturb the formation temperature around a borehole. The heat transfer associated with the mass movement (e.g., mud circulation, mud infiltration into formation, borehole cave-in, and formation fluid flow) is fairly complicated. Common practices that use transient borehole temperature for estimating the undisturbed formation temperature tend to be based on simplistic, analytic thermal recovery models because temperature data are usually noisy and sparse, caused in part by drilling disruptions or other borehole experiments. For heat flow measurement or temperature-related reservoir assessment, it is desirable to determine accurately the equilibrium formation temperature from the disturbed transient borehole temperature data.

Many studies based on transient bottom-hole temperature (BHT) have been reported. Deming (1989) comprehensively reviews the quality of BHT data, notes potential pitfalls of using a well-known method (Horner plot) for estimating equilibrium temperature from BHT, discusses the limits of using empirical relations to correct BHT, cites examples of using BHT in basin studies (Majorowicz and Jessop, 1981; Drury, 1984; Reiter et al., 1986; Deming and Chapman, 1988), and discusses the practicality of using more realistic heat-transfer models (Lee, 1982; Luheshi, 1983; Shen and Beck, 1986). Most BHT studies originate from oil and gas wells, and the data are usually collected before the bottom hole is thermally stabilized (see examples of using BHT in Towend, 1997, 1999; Forster and Merriam, 1999; Majorowicz et al., 1999). Rarely are BHT data precisely timed to within a few minutes or measured to be better than a few hundredths of a degree. The sparseness of data and uncertainty in data quality have prevented the development of a sophisticated thermal model for estimating formation temperature.

We present a method for determining equilibrium temperature and thermal conductivity from a series of thermal recovery data in boreholes. Through a test study on field data, subject to the limits of data quality and quantity, we also attempt to address the uncertainty of models that fit the data well and propose two measures in addition to rms misfits for assessing modeling results.

Here, the thermal recovery is simulated with a finite-element method that can handle a borehole filled by mud which is distinct from the formation in thermal properties. Thermal properties, equilibrium formation temperature, and their uncertainties will be determined using a quasi-linear inversion method that relies on a genetic algorithm to provide estimates of thermal properties as well as the initial and boundary conditions. Before the methodology is presented and the test results are discussed, we first review common methods of estimating

Manuscript received by the Editor September 5, 2002; revised manuscript received March 25, 2003.
*University of California, Department of Earth Sciences, Riverside, California 92521. E-mail: tien.lee@ucr.edu.
‡Institute of Geophysics, Siberian Branch of Russian Academy of Sciences, Prosp. Akad. Koptyuga 3, Novosibirsk, 630090 Russia. E-mail: duch@viggm.nsc.ru.

formation temperature from the transient borehole data and then forge those existing simplistic, analytic solutions into one equation which explains the observation (Deming, 1989) that the estimates by various methods appear to converge eventually to one value. We justify why one of those methods is chosen to help constrain our inverse modeling.

RELATIONS BETWEEN EXISTING METHODS

Various empirical relations between equilibrium formation temperature and BHT are excluded from consideration because those relations apply only to areas where relations were established and equilibrium temperatures used to construct those empirical relations were often dubiously described (Deming, 1989). Instead, we address universally applicable methods as follows.

Models of steady heat source

Two analytical solutions are commonly used for estimating formation temperature. The first is based on line source theory. Simulated as a heat sink for the cooling effect of mud circulation, the line source exchanges energy steadily with the formation (Bullard, 1947; Lachenbruch and Brewer, 1959). Essentially, the method assumes that the temperature disturbances are caused by a steady line source of finite cooling duration. According to the line source solution (Carslaw and Jaeger, 1959, p. 262) and the principle of linear superposition, the transient temperature $\theta(t)$ in the borehole behaves asymptotically:

$$\theta(t) \approx \theta_{asy} + \frac{Q}{4\pi k_{asy}} \ln \frac{t}{t - t_D}, \qquad (1)$$

where θ_{asy} is the asymptotic formation temperature, t is the time since the drill bit first touched the depth in question, t_D is the duration of mud circulation, Q is the steady rate of heat exchange per unit line length ($Q < 0$), and k_{asy} is the asymptotic thermal conductivity of the formation. (See Table 1 for notations and units.) The postdrilling time $t - t_D$ is commonly known as the shut-in time. A linear regression of $\theta(t)$ versus $\ln[t/(t - t_D)]$ yields intercept θ_{asy} and the slope for the Q/k_{asy} ratio. Usually this Q is not estimable; but if it is as demonstrated in this paper, k_{asy} can be found accordingly.

We review several methods for estimating formation temperature and conductivity. To distinguish various values obtained by different methods, we define asymptotic as a determination by equation (1). Hence, an asymptotic conductivity does not imply it is a time-dependent property.

The linear relation in equation (1) is commonly known as Lachenbruch's plot, which is equivalent to the Horner plot for pressure recovery in reservoir tests or to a drawdown recovery plot in aquifer pumping tests; here it is referred to as the steady heat-source model. Its principle can be implemented for in-situ thermal conductivity measurements in sediments with a given, steady line source Q. This asymptotic approximation is good to within 1% from the exact line source solution if $r^2/4\kappa(t - t_D) \leq 0.01$, where r is a characteristic distance (e.g., a borehole radius) and κ is the thermal diffusivity. As an example appropriate for our field test data ($\kappa \approx 0.3 \times 10^{-6}$ m^{2}s^{-1} and $r \approx 0.1$ m), the shut-in time $t - t_D$ should be greater than 230 hours for a desired 1% accuracy.

Models of steady circulating mud temperature

The other commonly used analytic solution is based on the assumption that the temperature $\theta(t)$ in a borehole of radius a drops instantly from the formation temperature θ_f to an unknown, initial mud temperature θ_m (Carslaw and Jaeger, 1959, p. 260):

$$\frac{\theta(t) - \theta_m}{\theta_f - \theta_m} = \exp\left(-\frac{a^2}{4\kappa t}\right). \qquad (2)$$

Table 1. Notations

Symbol	Definition
a	$= r_w$, borehole radius, m
A	all shifted data
BHT	bottom-hole temperature
$\mathbf{c}^e$	capacitance matrix, element
$\mathbf{C}$	capacitance matrix, global
$\mathbf{C}_d$	covariance matrix, data
$\mathbf{C}_p$	covariance matrix, parameters
$\mathbf{C}_{p'}$	post processing $\mathbf{C}_p$
$\mathbf{d}$	computed temperature, °C
$\mathbf{d}^{obs}$	observed temperature, °C
D	diffusion distance
E	early time data
f	$= \theta_{asy}/\theta_{equ} - 1$
FE	finite element
$\mathbf{G}$	sensitivity matrix
GA	genetic algorithm
IM	inverse modeling
k	conductivity, Wm^{-1}K^{-1}
k_1	k, borehole
k_2	k, sediment
k_{asy}	k, asymptotic
k_s	k, instant heat release
$\mathbf{k}^e$	conductance matrix, element
$\mathbf{K}$	conductance matrix, global
L	late data
M	number of parameters
N	number of data points
N_r	number of elements
$\mathbf{p}$	parameter vector
$\mathbf{p}^{guess}$	guessed $\mathbf{p}$
Q	heating rate/length
Q^{tot}	total heat release/length
r	radial distance, m
r_w	borehole radius, m
r_∞	radius of model domain
rms	root means squares, °C
S	objective function
S^I	S, data and parameters
S^{II}	S, constrained by $\theta_{asy}/\theta_{equ}$
t	time since drilling, s
t_D	duration of mud circulation
t_{end}	t at last observation
w	weighting factor for S^{II}
Δt	time step duration
θ	temperature, °C
θ^n	θ at nth iteration
θ_1	θ, borehole
θ_2	θ, sediment
θ_{asy}	θ_∞, asymptotic relation
θ_{equ}	θ_∞, GA-IM model
θ_f	θ_∞, zero circulation model
θ_m	θ, mud
θ_∞	equilibrium formation θ
$\Delta\theta$	$\theta_{asy} - \theta_{equ}$
κ	thermal diffusivity, m^{2}s^{-1}
ρc	heat capacity, Jm^{-3}K^{-1}

The mud and formation are considered to have the same thermal properties. We call this relation the zero circulation model, a special case for models of steady circulating mud temperature. By iteratively modifying θ_m to maximize the linear correlation of $\ln[(\theta(t)-\theta_m)/(\theta_f-\theta_m)]$ versus $1/t$, one can determine κ, then find θ_f from equation (2). This and similar approximations for cases of constant circulating mud temperature have been used to estimate formation temperature from BHT measured after mud circulation has ceased (Middleton, 1979; Leblanc et al., 1981; Jones et al., 1984).

Equation (2) has been improved with analytical or numerical solutions by considering mud circulation of finite duration at constant temperature and a borehole filled by mud with distinctive thermal properties (Lee, 1982; Luheshi, 1983). The accounting of borehole property allows the use of short-term temperature measurements to estimate formation temperature; the implementation of finite mud circulation time permits estimates at any depth where zero circulation time is not an appropriate assumption. The improvement has been advanced further by Shen and Beck (1986) and Cao et al. (1988) to include the effect of radial or lateral fluid flow.

Models of instant heating

Being a variant to the steady-line source solution in equation (1), a third relation based on instantaneous heat release has been used frequently to obtain equilibrium temperature from the cooling history of a temperature sensor probe that was frictionally heated during its rapid insertion into unconsolidated sediments to measure geothermal gradient and hence heat flow through the ocean or lake floor (Hutchison and Owen, 1989). At large time values the temperature at the source location evolves like (Carslaw and Jaeger, 1959, p. 258)

$$\theta(t) \approx \theta_f + \frac{Q_{tot}}{4\pi k_s t}, \tag{3}$$

where Q_{tot} is the total frictional heat production per unit line length ($Q_{tot} > 0$) and k_s is the thermal conductivity of a homogeneous medium. In contrast to equation (1), this is named the instant heating model. The equilibrium temperature θ_f is obtainable from a linear regression of $\theta(t)$ versus $1/t$, but k_s is indeterminable from the regression-line slope because Q_{tot} is unknown.

Lee and von Herzen (1994) use the initial temperature rise resulting from frictional heating, instead of heat production Q_{tot}, to simulate a thermal probe's cooling history and to inverse model the observed transient temperature for estimating equilibrium temperature and thermal conductivity. Lee et al. (2003) estimate Q_{tot} from inverse modeling and use the resultant Q_{tot} to obtain k_s in accordance with equation (3). This k_s is expected to equal the conductivity k derived by the inverse modeling. Hence $3(k_s/k-1)^2$ was added to the conventional misfit function for inverse modeling. The equilibrium temperature θ_{equ} resulted from the k_s/k-constrained inverse modeling is then compared with the independently obtained θ_f as one of several measures for assessing the modeling results.

The method based on the model of steady circulation mud temperature (Lee, 1982) has been modified and applied to borehole data in Lake Baikal to estimate equilibrium temperature and thermal conductivity (Duchkov et al., 2001). The resultant conductivity values agree to within 10% of the values obtained with a commonly practiced needle probe method (based on a steady line source method described originally by von Herzen and Maxwell, 1959) for unconsolidated sediments but deviate more than 50% from the values obtained with a thermal comparator (based on calibration with reference material; Kalinin et al., 1983; Duchkov, 1991; also see a hybrid method by Lee, 1989).

Model equivalency

Now we are ready to show that, to the first-order approximation, equations (1)–(3) are equivalent at large time values. The steady heat-source model in equation (1) for $t \gg t_D$ becomes

$$\theta(t) = \theta_{asy} - \frac{Q}{4\pi k_{asy}} \ln\left(1 - \frac{t_D}{t}\right) \approx \theta_{asy} + \frac{Qt_D}{4\pi k_{asy} t}, \tag{4}$$

which is equivalent to equation (3) for the instant heating model because Qt_D is the total heat exchange per unit line length during mud circulation ($Qt_D < 0$). For this relation of θ versus $1/t$ to be applicable, the ratio t_D/t must be less than 0.2 for the slope to be determined to within 10%, or 0.1 for 5%. Most of our test data do not satisfy the t_D/t conditions. Hence, equation (1) is the choice for the modeling constraint.

If the term $\exp(-a^2/4\kappa t)$ in equation (2) for the model of zero circulation time is replaced by $(1-a^2/4\kappa t)$ for small $a^2/4\kappa t$ at large time values, equation (2) becomes

$$\theta(t) \approx \theta_f + \frac{-\pi a^2 \rho c(\theta_f - \theta_m)}{4\pi k t} \tag{5}$$

by noting that $\kappa = k/\rho c$. This relation is again equivalent to equation (3) because the factor $-\pi a^2 \rho c(\theta_f - \theta_m)$ represents the total heat energy exchange per unit line length ($\theta_f > \theta_m$). The needed waiting time for equation (5) to be applicable is proportional to the borehole's cross-sectional area.

The equivalency in equations (3), (4), and (5) explains why the estimates of equilibrium temperature by different methods or recovery models tend to converge at large time. Hence, consistency in the estimates of formation temperature by the three different methods is necessary but insufficient to validate any estimates.

We revisit the data from Lake Baikal and add a genetic algorithm to improve the selection of trial parameter values for inverse modeling. Many sets of inversion results, of which the rms of misfits between the observed and computed temperatures are on par with the level of measurement errors, can be generated to define the uncertainty of parameter determinations. Furthermore, as an option, the difference between the simulated θ_{equ} and the θ_{asy} of equation (1) can be imposed as an additional term $(\theta_{asy}/\theta_{equ}-1)^2$ in the misfit function for inverse modeling. The steady heat exchange rate Q in equation (1) is also estimated by modeling to yield a k_{asy} that can then be compared with the k determined by inverse modeling as an additional check for confidence in the results of modeling.

THERMAL RECOVERY MODELING

Modeling thermal recovery in a borehole that has been cooled by mud circulation consists of two intertwining phases: (1) forward modeling computes temperature distribution from the given initial and boundary conditions and material properties, while (2) inverse modeling revises the conditions and properties in view of the given borehole recovery data.

Governing equation and conditions

By inspecting the transient borehole temperature variations, we assume thermal recovery was dominated by heat conduction. Neglecting the vertical heat transfer, of which the rate is much smaller than the radial flow rate, the heat conduction for an axisymmetric problem follows:

$$\frac{\partial^2\theta}{\partial r^2}+\frac{1}{r}\frac{\partial\theta}{\partial r}=\frac{\rho c}{k}\frac{\partial\theta}{\partial t}, \tag{6}$$

where $\theta(r,t)$ is temperature, r is radial distance, t is time, k is thermal conductivity, and ρc is volumetric heat capacity, which is a product of mass density ρ and specific heat c.

The thermal regime consists of two media with distinctive thermal properties k and ρc, one inside the borehole (medium 1) and the other outside. Initially the temperature in the two media is uniform at θ_{equ}, i.e.,

$$\theta_1(r,0)=\theta_2(r,0)=\theta_{equ}. \tag{7}$$

Mud starts to circulate at the depth of interest in the borehole at time 0. The borehole temperature remains at θ_m for a duration of t_D, and the far-field temperature stays forever at θ_{equ}. Explicitly, the boundary conditions are

$$\begin{aligned}&\theta_1(r,t)=\theta_m, && 0\le t\le t_D;\\ &\left(\frac{\partial\theta_1}{\partial r}\right)_{r=0}=0, && t_D<t<\infty;\\ &\theta_2(\infty,t)=\theta_{equ}, && 0\le t<\infty.\end{aligned} \tag{8}$$

The condition of $\partial\theta_1/\partial r=0$ at $r=0$ implies that no heat energy is extracted from or injected into the borehole after mud circulation stops, except for the heat exchange through the borehole interface. The conditions at the interface $r=r_w$ for all time are

$$\begin{aligned}&\theta_1(r_w,t)=\theta_2(r_w,t),\\ &\left(k_1\frac{\partial\theta_1}{\partial r}\right)_{r_w}=\left(k_2\frac{\partial\theta_2}{\partial r}\right)_{r_w}.\end{aligned} \tag{9}$$

The thermal recovery is now fully described by the governing differential equation as well as the initial and boundary conditions, provided that seven parameters including k_1, $(\rho c)_1$, k_2, $(\rho c)_2$, θ_m, θ_{equ}, and t_D are known. The solution is obtained through a finite-element method.

Finite-element analysis

Given these seven parameters, one can simulate the borehole temperature and compare it with the observed temperature. Here the simulation as forward modeling is based on 1D axisymmetric finite-element analysis, for which theoretical development is available in several texts (e.g., Bathe and Wilson, 1976). The relevant formulation is given below.

The region of interest between $r=0$ and $r=r_\infty$ (r_∞ is a proxy of infinite radial distance ∞) is discretized into N_r ring (shell) elements with the ring thickness increasing radially outward. The radius of the innermost ring coincides with the borehole radius r_w, which may be enlarged to account for borehole cave-in if necessary. The outermost ring radius r_∞ is at least five times the conduction distance $D=\sqrt{\kappa t_{end}}$, where t_{end} is the ending observation time, counting from the time when the drill bit first touches the depth of temperature observation. This choice of r_∞ ensures that the nodal temperatures at five or more outer nodes are at θ_{equ}. The number of rings N_r and ring thicknesses are estimated empirically.

The medium outside the borehole is presumed to be homogeneous and isotropic, and its thermal properties differ from those of the water–mud-filled borehole. The properties are also assumed to be independent of temperature for the range considered (~2–10°C).

The temperature inside each element is interpolated linearly between its two bounding nodal temperatures. The nodal temperature at r_∞ stays at θ_{equ}. During mud circulation ($t\le t_D$), the nodal temperatures at $r=0$ and $r=r_w$ are maintained at θ_m; but for $t>t_D$, the two are allowed to vary by switching the constant-temperature condition for $r\le r_w$ to zero heat flux condition at $r=0$ (i.e., $\partial\theta/\partial r=0$).

After minimizing the Galerkin weighted residual and using linear interpolation for temperature distribution between two consecutive time steps, the governing equation (6) and the initial and boundary conditions become a set of simultaneous equations for nodal temperature vector θ^{n+1} at time $(n+1)\Delta t$ in terms of θ^n at time $n\Delta t$:

$$\left(\mathbf{C}+\frac{2\Delta t}{3}\mathbf{K}\right)\boldsymbol{\theta}^{n+1}=\left(\mathbf{C}-\frac{\Delta t}{3}\mathbf{K}\right)\boldsymbol{\theta}^{n},\quad n=0,1,2,\ldots. \tag{10}$$

The $(N_r+1)\times(N_r+1)$ global capacitance matrix $\mathbf{C}$ is assembled from the 2×2 elementary matrix,

$$\mathbf{C}^e=\frac{\rho c\bar{r}\,\Delta r}{6}\begin{bmatrix}2&1\\1&2\end{bmatrix}. \tag{11}$$

The global conductance matrix $\mathbf{K}$ is similarly assembled from the elementary matrix

$$\mathbf{K}^e=\frac{k\bar{r}}{\Delta r}\begin{bmatrix}1&-1\\-1&1\end{bmatrix}, \tag{12}$$

where $\bar{r}$ is the mean of the outer and inner radii of element e, Δr is its ring thickness, and the k and ρc are properties of element e.

In the first time step, the $(N_r+1)\times1$ column vector $\boldsymbol{\theta}^0$ represents the initial condition; $\boldsymbol{\theta}^1$ is the final nodal temperature, obtained by means of the Gaussian elimination procedures. In the second time step, $\boldsymbol{\theta}^1$ plays the role of initial temperature for obtaining a set of new nodal temperatures $\boldsymbol{\theta}^2$. The process cycles through all time steps. The step size Δt is generally a fixed fraction of the least sampling interval.

Inverse modeling

For inverse modeling to determine the model-defining parameters, we apply an iterative Newton-Gauss method to a scalar objective function or misfit function:

$$\begin{aligned}S&=S^I+wS^{II},\quad w=0\ \text{ or }\ 1,\\ S^I&=\frac{1}{2}\Big\{\left(\mathbf{d}^{obs}-\mathbf{d}\right)^T\mathbf{C}_d^{-1}\left(\mathbf{d}^{obs}-\mathbf{d}\right)\\ &\quad+(\mathbf{p}^{guess}-\mathbf{p})^T\mathbf{C}_p^{-1}(\mathbf{p}^{guess}-\mathbf{p})\Big\},\\ S^{II}&=\frac{1}{2}\left(\frac{\theta_{asy}}{\theta_{equ}}-1\right)^2,\end{aligned} \tag{13}$$

where S^I defines a misfit between observed and computed temperatures as well as between guessed and modeled parameters (Tarantola, 1987; Lee, 1999), S^{II} measures the closeness between θ_{asy} and θ_{equ}, and weighting factor w dictates whether the constraint S^{II} is imposed; $\mathbf{d}^{obs}$ is the $N \times 1$ observed borehole temperature vector, $\mathbf{d}$ is the $N \times 1$ temperature vector (i.e., $\boldsymbol{\theta}$ at $r = 0$) computed from the desired parameter vector $\mathbf{p}$, $\mathbf{p}^{guess}$ is the $M \times 1$ guessed values of parameter vector, $\mathbf{C}_d$ is the $N \times N$ covariance matrix of data, $\mathbf{C}_p$ is the $M \times M$ covariance matrix of parameters, N is the number of the observed temperature data points, and M is the number of parameters. The superscript T designates the transpose of a matrix. The diagonal entries of $\mathbf{C}_d$ and $\mathbf{C}_p$ are the variances of the data and parameters, respectively. The differences between $\mathbf{d}^{obs}$ and $\mathbf{d}$ and between $\mathbf{p}^{guess}$ and $\mathbf{p}$ are assumed to have Gaussian distributions. The data are also assumed to have random errors but no systematic error. The parameters are theoretically independent of one another for a given material such that the off-diagonal entries for the two covariance matrices are set to zero initially. (The postprocessing $\mathbf{C}_p$ is not necessarily diagonal, implying some crosscorrelation among the parameters or numerical dispersion in our test examples.)

Minimization of S with respect to $\mathbf{p}$ (i.e., setting $\partial S/\partial \mathbf{p} = 0$) and solving for $\mathbf{p}$ from the resultant simultaneous equations yield the iterative relation,

$$\mathbf{p}_{i+1} = \mathbf{p}^{guess} + \mathbf{C}_{p'i}\mathbf{G}_i^T\mathbf{C}_d^{-1}\{(\mathbf{d}^{obs} - \mathbf{d}_i) - \mathbf{G}_i(\mathbf{p}^{guess} - \mathbf{p}_i)\} - \mathbf{C}_{p'i}\, f_i \frac{\partial f_i}{\partial \mathbf{p}_i}, \tag{14}$$

where i is the iteration step and

$$f_i = \frac{\theta_{asyi}}{\theta_{equi}} - 1. \tag{15}$$

Others symbols will be explained shortly. Equation (14), excluding the f-bearing term, is given by Tarantola (1987) and Lee (1999, equation 10.75). The entries of the $N \times M$ sensitivity matrix $\mathbf{G}_i$ are defined by

$$G_{i,nm} = \left.\frac{\partial d_n}{\partial p_m}\right|_{\mathbf{p}_i}, \quad n = 1, 2, \ldots, N; \quad m = 1, 2, \ldots, M. \tag{16}$$

This partial derivative is evaluated numerically at the nth computed borehole temperature and at iteration step i. Matrix $\mathbf{C}_{p'i}$ is the postprocessing covariance matrix, which is reciprocal to the Hessian:

$$\mathbf{C}_{p'i}^{-1} = \mathbf{C}_p^{-1} + \mathbf{G}_i^T\mathbf{C}_d^{-1}\mathbf{G}_i. \tag{17}$$

The derivatives $\partial f_i/\partial \mathbf{p}_i$ are evaluated for the θ_{equ} and t_D variations only because the intercept θ_{asy} is obtained from the regression analysis of the asymptotic relation, equation (1), which depends solely on t_D. The asymptotic conductivity k_{asy}, however, depends on the slope through heating rate per unit line length Q, which is computed from the temperature disturbance at the end of mud circulation:

$$Q = \frac{2\pi}{t_D}\int_0^\infty \rho c\,[\theta(r, t_D) - \theta_{equ}]\, r\, dr, \tag{18}$$

where $\theta(r, t_D)$ is linearly interpolated between nodal temperatures.

As a footnote, Lee et al. (2003) use $(k_s/k - 1)^2/2$ as the S^{II} constraint (instant heating model) instead of $(\theta_{asy}/\theta_{equ} - 1)^2/2$ (steady heat-source model) because their primary inverse modeling objective is to determine thermal conductivity in situ, while we mainly estimate formation temperature.

Fitting criteria.—Four measures are used to select the inverse modeling results. The misfit between $\mathbf{d}^{obs}$ and $\mathbf{d}$ is first assessed by the rms:

$$\text{rms}_1 = \sqrt{\frac{1}{N}\sum_{n=1}^{N}\left(1 - \frac{d_n}{d_n^{obs}}\right)^2},$$

$$\text{rms}_2 = \sqrt{\frac{1}{N}\sum_{n=1}^{N}(d_n^{obs} - d_n)^2}. \tag{19}$$

Generally, rms_1 shows greater resolution than rms_2 for our test examples; therefore, the former is the preferred measure. However, rms_2 is still monitored because rms_2 can be compared directly with the data error. For each choice of $\mathbf{p}^{guess}$, there is a minimum in rms among all iterations i. Since there are a countless number of local minima in the seven-parameter model space, one assignment of $\mathbf{p}^{guess}$ may not lead to the desired global minimum, which is found by using a genetic algorithm to generate numerous $\mathbf{p}^{guess}$.

The parameters $\mathbf{p}$ that yield the least rms among the minima in rms for all choices of $\mathbf{p}^{guess}$ are generally the preferred model parameters in the belief that the associated rms is at the global minimum. However, in view of our data quality and uncertainty in modeling cooling behavior during mud circulation and subsequent thermal recovery, the parameters $\mathbf{p}$ associated with the least rms may not be the correct choice. The misfit distribution $(\mathbf{d} - \mathbf{d}^{obs})$ is hence included as a second measure, with the understanding that those distributions are not compared, quantitatively. The third measure is the difference between θ_{equ} and θ_{asy}, regardless of whether the optional constraint S^{II} is imposed for the inversion. The fourth measure checks the oneness in the ratio of k_{asy} to k. This fourth measure can be imposed directly in inverse modeling, but it has not been implemented because (1) the ratio is intentionally excluded for an independent assessment of the model k and (2) depending on the range of time used in modeling, the S^{II} may not be applicable and the addition of conductivity ratio could obliterate the inverse modeling.

The four measures are compatible with one another if a good numerical model is found. As described later, only a few test results can satisfy all four measures. Hence, we present the averages for all test results, assign the standard deviations as the uncertainties, and use the discrepancy $\theta_{asy} - \theta_{equ}$ and ratio k_{asy}/k to assess the results.

Genetic algorithm

The results of inverse modeling vary with $\mathbf{p}^{guess}$. The outcome can be modified by iteratively fine-tuning the input values, as done in Duchkov et al. (2001), in which the third and fourth measures of curve fitting were not exercised. Manual fine-tuning is tedious and is subject to a modeler's intuition and bias. Before the fine-tuning stage is reached, inverse modeling may suffer numerous run-time crashes. A genetic algorithm is

thus implemented to achieve reasonably objective results. Genetic algorithm coding is problem dependent (Lee et al., 2001); hence, only a brief accounting of the coding is described.

The genetic algorithm begins with N_{GA} randomly selected sets of parameter values, every one of which is within a defined range for each parameter. Misfits are computed for all sets according to equation (19). Among them, the least rms is found, and the standard deviation of all rms is computed. The parameter sets whose rms lies beyond 0.4β from the least rms are rejected, where $\beta = (\text{rms}_{average} - \text{rms}_{least})$ and $\text{rms}_{average}$ is the average rms for the N_{GA} sets of parameter values. The cutoff (0.4β) is empirically selected such that about 10% or more of the population can survive in the early stage of evolution. The surviving parents give birth to the offspring to replace the perished individuals, keeping the population at the same N_{GA} for every generation.

The offspring are generated by one of the four randomly selected procedures: retaining a surviving parent without modifying any of its parameter values, exchanging some parameter values between two parents, taking weighted mean values for some parameters of two parents, and perturbing some parameter values of a surviving parent. The perturbation allows an opportunity to move away from a local minimum in the parameter space.

The reproduction processes are iterated for 15 generations; a minimum in rms for each generation is identified. The least among those 15 minima is $\mathbf{p}^{guess}$, which is then input to the inverse model. Each $\mathbf{p}^{guess}$ yields a set of model parameters $\mathbf{p}$. The sequence of genetic algorithm and inverse modeling for a given data set is typically repeated five to ten times to find the potential ranges or uncertainty for each of the parameter determinations.

With some modifications, the above-mentioned basic genetic algorithm structures are applicable to other inverse problems. For example, Lee et al. (2002) use genetic algorithm and inverse modeling in the logarithmic space of parameters (instead of a linear scale here) to determine hydraulic properties in an unconfined aquifer.

TEST EXAMPLES

The genetic algorithm/inverse modeling/finite element (GAIM-FE) sequence is tested with two data sets, BDP93 (Baikal Drilling Project–1993) and BDP96, from three boreholes in Lake Baikal, Russia. This testing is supplemented with synthetic data to cast some light on our methodology as applied to real data.

The BDP93 set (Duchkov and Kazantsev, 1996) consists of temperature measurements from two boreholes located a few meters apart in the Buguldeika saddle (52°32′N, 106°08′E). The early part (12–50 hours postdrilling, Figure 1) of BDP93 came from a hole drilled through an ice sheet to 95 m below the lake floor beneath a water depth of 355 m. It took about 200 hours to complete the drilling, and the hole was flushed with lake water (∼ 1°C). The sediments are mainly unconsolidated, alternating biogenic (diatomaceous) and terrigenous muds (water content ∼40%). A thermal logging cable with three thermistor sensors spaced at 30-m depth intervals was installed after the drilling, and the thermal recovery was recorded from 12 to 50 hours and reported to the nearest hour. The late part of BDP93 (76 to 380 hours) came from another hole that was actually drilled first and took ∼300 hours to drill to a depth of 100 m. An unnatural transition appeared in the merged temperature–time trend (Figure 1). Hence, the two segments were aligned by eyeball to yield a smooth temperature transition between 50 and 76 hours postdrilling (Figure 2). The tests for this study were conducted for the two parts separately and for the entire realigned data set.

Borehole BDP96 was drilled to a depth of 100 m in about 110 hours below a water depth of 320 m in the Academichesky Ridge (53°42′N, 108°21′E). The temperature was recorded between 100 and 193 postdrilling hours. The logging cable slipped between 166 and 170 hours (Figure 3). For modeling purposes, the temperature data after 170 hours are migrated downward by a constant amount for each sensor, again by eyeball aligning the segmented data.

As described earlier, the drilling and temperature recordings did not indicate a smooth, ideal operation: the duration of mud circulation is uncertain, the recording timing is good to one-half hour, and the mud temperature is likely to have

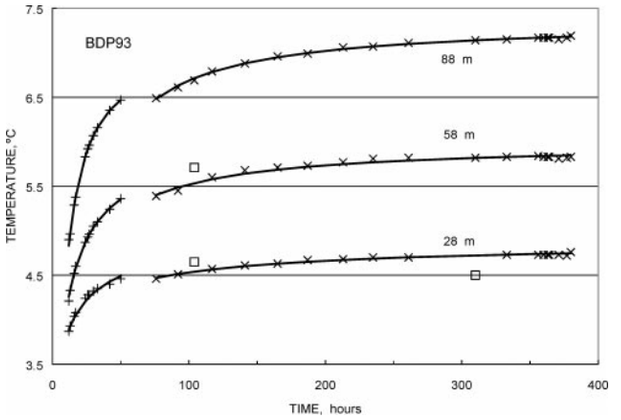

FIG. 1. Thermal recoveries at three depths at site BDP93 in Lake Baikal, Russia. Each curve represents one set of model parameters. Outliers (□) are excluded from modeling. The early (postdrilling time ≤ 50 hours) and late data sets were obtained from two boreholes spaced a few meters apart. Data are marked by + or ×.

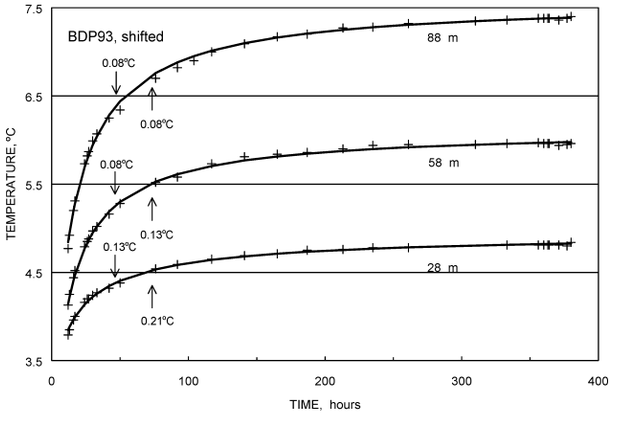

FIG. 2. Model curves of thermal recovery at BDP93. Data were merged from two boreholes through eyeball alignment of two segments of temperature–time data (Figure 1). The number next to each arrow indicates the amount of temperature shift that has been made for the alignment. Data are marked by +.

fluctuated substantially. For our modeling, the recording is assumed to be accurately timed; the unsteady mud temperature is higher than the flushing water temperature and is assumed to be constant at each depth of measurement. The data error is probably within $\pm 0.05^{\circ}$C as judged by the smoothness of the thermal recovery curves, uncertain time resolution, and existence of three outliers in the data. This error estimate sets the limit of goodness in curve fitting. Ranking numerical models in genetic algorithm and inverse modeling is based on rms_1 (rms_2 lacks comparable resolution). Here, all results with rms_2 below 0.06°C are deemed acceptable in terms of misfit rms alone. This target misfit limit is much greater than the limit (0.002°C) used in a study by Lee et al. (2003), who apply a similar but not identical method [e.g., equation (1) instead of equation (3)] to high-quality data to determine formation temperature and thermal properties in the top 2 m of Lake Baikal sediments. The present study tests the general methodology with comparatively inferior data sets, which in practice could be frequently encountered.

Implementation

We implemented our test examples as follows.

Finite-element simulation.—The forward finite-element modeling of BDP93 is based on a domain size of 8.1 m radius. This is discretized into 32 ($= N_r$) elements, with their widths increasing radially from the innermost element of 0.12 m (radius of borehole) to 0.30 m for the outermost one. For BDP96 and the early segment of BDP93, the N_r is reduced to 28 and the domain size is 6.9 m. These two choices ensure that, at the end of temperature recording (drilling plus postdrilling time), the nodal temperatures at five or more outer nodes equal the far-field equilibrium temperature θ_{equ}. The square of the presumed data error $(0.05^{\circ}\text{C})^2$ is taken as the variance in the data covariance matrix $\mathbf{C}_d$, and the square of 10% of $\mathbf{p}^{guess}$ is taken as the variance for the respective parameter in $\mathbf{C}_p$. The borehole temperature is computed as the average of the nodal temperatures, weighted by a 2:1 ratio, at the center and edge of the borehole.

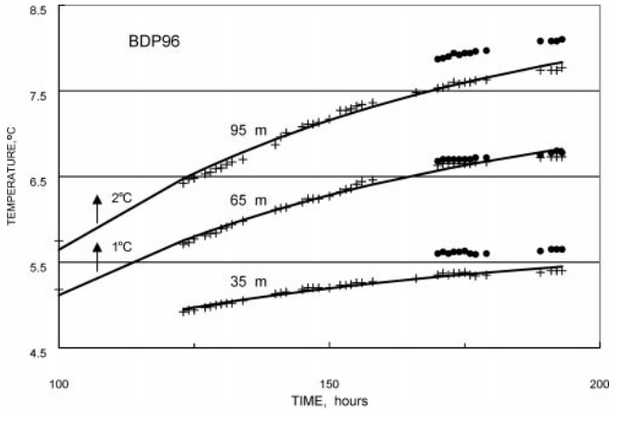

FIG. 3. Thermal recoveries at site BDP96 in Lake Baikal, Russia. The original data marked by dots have been downshifted by eyeball alignment with the pre-170 hours data for modeling. The entire data set and curve at depths 65 and 95 m have been subtracted by 1° and 2°C, respectively, for plotting. Data used for modeling are marked by +.

The basic time step Δt used in the finite-element model is either one-half or one-third of the shortest sampling interval. The two choices do not lead to a significant difference in results. Either choice of Δt may be slightly reduced such that the temperature is computed exactly at each observation time. Essentially, a variable Δt is used in the finite-element model.

Parameter ranges.—The genetic algorithm is initiated by the modeler with a pseudorandom number. It then randomly selects 100 ($= N_{GA}$) sets of parameters from the following ranges of choice: The conductivity values for the sediments range from 0.8 to 1.5 $\text{Wm}^{-1}\text{K}^{-1}$, and heat capacity values range from 1.0 to 3.0×10^6 $\text{Jm}^{-3}\text{K}^{-1}$ (the corresponding ranges for the mud properties are 2∼4 and 0.15∼0.9 units, respectively). The lower bound of the mud temperature is the inlet lake water temperature (1°C), and its upper bound is the zero-time intercept of a linear relation obtained for the first four data points. The equilibrium temperature uses the mean of the last two temperature readings as its lower limit and adopts a range twice that between the lower limit and a θ_f obtained from the last four readings according to equation (3). Because the temperature–time curve is concave downward (Figure 1), such chosen ranges for the mud temperatures are relatively large for the late data segments as compared to those for the early segments at site BDP93; the reverse is true for the potential range of equilibrium temperature.

The mud circulation time t_D, which ostensibly should be the least uncertain to estimate from the drilling records, has the largest uncertainty because t_D is not necessarily the interval between the time when the drill bit first touches the depth of temperature measurements and the time when drilling ends. After drilling, the mud may continue to circulate for some time, posing a challenging game of estimating t_D. For BDP96, the ranges are narrow because the time the drill bit first passed the depth in question is available; but for BDP93, such information is not available, and the likely ranges are relatively wider. The ranges and the midrange values of t_D decrease with increasing depth. For a given depth, the t_D is also greater for the late segments than for the early segments because it took about 1.5 times longer to drill the hole for the late segment. For the composite data sets, the t_D ranges straddle those for the early and late segments.

Selection.—Fifteen generations are allowed in genetic algorithm for every chosen pseudorandom number. The population in each generation is kept at 100 sets. Misfit is computed for each set; the minimum among those misfits (rms_1) is the misfit for that generation. The set of parameters associated with the least among the 15 generational minima constitute $\mathbf{p}^{guess}$. After an initial rapid decline in rms_1, increasing the number of generations beyond 15 does not improve rms_1 significantly.

No parameter ranges are imposed during inverse modeling [equation (14)], which begins with the input of $\mathbf{p}^{guess}$ from genetic algorithms. The resultant $\mathbf{p}$ is regarded as a desired set of parameter values if the accompanying rms_2 is less than 0.06°C. Usually, $\mathbf{p}$ does not differ much from $\mathbf{p}^{guess}$. Occasionally, the output $\mathbf{p}$ is identical with the input $\mathbf{p}^{guess}$ to three significant digits, but in those cases inverse modeling is still capable of yielding slightly better misfit distributions. Rarely, inverse modeling crashes with the input provided by genetic algorithms. Multiple

runs generate a set of **p**, almost all of whom meet the rms_2 criterion. The arithmetic means of those rms_2-passed **p** are taken as the final parameter values, and their standard deviations signify the uncertainty of determination.

Remarks.—The linearity of equation (1) is obtained at each inverse modeling-estimated t_D by maximizing its linear correlation coefficient through one-by-one removal of the earlier data points until at least five points remain or a correlation coefficient of 0.98 or better is achieved. Usually, high linearity is achieved after a few points have been skipped, but occasionally the removal of up to 20 points may be needed. The intercept θ_{asy} and the slope $Q/4\pi k_{asy}$ are obtained from the linear relation with the highest correlation coefficient.

Depending on the PC's clock speed, the run time for each GA-IM-FE sequence is about 5 to 10 minutes. The inverse modeling run time is only a small fraction of the total run time. The genetic algorithm as a means of solving the governing differential equation can produce the desired rms_2, but the addition of inverse modeling yields better fitting distribution in the sense of least squares.

Results

The results of curve fitting, without the constraint of S^{II} in equation (13), are illustrated in Figure 1 for every segment of BDP93. Three outliers marked by squares are excluded from modeling. Figure 2 exemplifies the fitting for the realigned composite data; the amounts of temperature shifting are posted next to the arrows.

Figure 3 depicts the results of modeling BDP96. The data marked by dots beyond hour 170 have been downshifted to correct for the offsets in the data curves caused by a cable slippage. Also, note that 1° and 2°C have been subtracted from the data and model curves, respectively, at 65 and 95 m depth for graphical accommodation.

Table 2 summarizes the results of modeling without the constraint of S^{II}: heat capacity, thermal conductivity, and formation temperature. The listed values are means ± standard deviations for five genetic algorithm/inverse modeling runs, except that the early segments at BDP93 were run 10 times each. Also tabulated are values that can be used to assess modeling results: ratios of asymptotic to model conductivity (k_{asy}/k), differences between asymptotic and model formation temperature ($\theta_{asy} - \theta_{equ}$), and misfits ($rms_2$). All modeling results with $rms_2 \leq 0.06$°C are summarized for the tabulation.

The uncertainties in determining formation temperature and conductivity are also illustrated in Figures 4 and 5, respectively. For every depth of measurement, there are two vertical bars for each: all composite (A), early (E), and late (L) data sets. Each upper bar in Figure 4 represents the equilibrium temperature, and each lower bar represents the difference $\theta_{asy} - \theta_{equ}$. Every bar centers at its mean value, and the height signals two standard deviations. The mean values are plotted with reference to the mean equilibrium temperature determined for the A data set at each depth of BDP93; the mean value for every A data set is then reset at 1°C for graphical comparison. Similarly, all equilibrium temperatures for BDP96 are reset to 1°C for comparison. The uncertainties in conductivity at each depth are also represented by two vertical bars (Figure 5), with the upper bar for conductivity and the lower one for the ratio k_{asy}/k.

Table 2. Results of modeling without the constraint of S^{II}. Numbers designate average ± one standard deviation.

	Heat capacity ($10^6 Jm^{-3}K^{-1}$)	Conductivity ($Wm^{-1}K^{-1}$)	Formation temperature (θ_{equ}, °C)	Conductivity ratio (k_{asy}/k)	Difference ($\theta_{asy} - \theta_{equ}$, °C)	rms_2* (°C)
BDP93†						
28 m						
Early	1.46 ± 0.31	1.35 ± 0.10	5.00 ± 0.06	1.51 ± 0.12	−0.23 ± 0.04	0.046 ± 0.002
Late	1.94 ± 0.56	1.24 ± 0.28	4.96 ± 0.01	1.09 ± 0.08	−0.01 ± 0.01	0.016 ± 0.001
All	1.48 ± 0.42	1.33 ± 0.13	4.95 ± 0.03	1.10 ± 0.10	−0.02 ± 0.02	0.027 ± 0.005
58 m						
Early	1.87 ± 0.50	1.26 ± 0.15	6.04 ± 0.06	1.24 ± 0.12	−0.15 ± 0.06	0.046 ± 0.009
Late	1.37 ± 0.47	1.29 ± 0.20	6.12 ± 0.01	0.85 ± 0.08	0.02 ± 0.02	0.031 ± 0.002
All	1.57 ± 0.41	1.30 ± 0.12	6.12 ± 0.01	1.05 ± 0.09	−0.01 ± 0.02	0.030 ± 0.003
88 m						
Early	2.11 ± 0.49	1.26 ± 0.07	7.04 ± 0.09	1.00 ± 0.09	−0.02 ± 0.04	0.031 ± 0.007
Late	1.86 ± 0.48	1.26 ± 0.09	7.57 ± 0.01	0.91 ± 0.04	0.02 ± 0.01	0.016 ± 0.001
All	1.81 ± 0.50	1.21 ± 0.17	7.56 ± 0.02	0.96 ± 0.08	0.02 ± 0.03	0.044 ± 0.003
Syn58	2.00	1.20	6.10			
Early	1.91 ± 0.64	1.21 ± 0.19	6.16 ± 0.09	1.19 ± 0.17	−0.13 ± 0.08	0.033 ± 0.005
Late	1.66 ± 0.59	1.26 ± 0.13	6.09 ± 0.01	0.95 ± 0.06	0.01 ± 0.01	0.023 ± 0.001
All	1.63 ± 0.52	1.19 ± 0.14	6.10 ± 0.02	1.04 ± 0.07	−0.01 ± 0.01	0.023 ± 0.002
BDP96**						
35 m	1.78 ± 0.48	1.00 ± 0.10	6.39 ± 0.08	0.71 ± 0.06	0.21 ± 0.05	0.029 ± 0.001
65 m	1.98 ± 0.23	0.95 ± 0.09	9.23 ± 0.07	0.43 ± 0.03	0.78 ± 0.05	0.047 ± 0.001
95 m	1.90 ± 0.76	0.90 ± 0.07	11.26 ± 0.14	0.33 ± 0.03	0.51 ± 0.04	0.058 ± 0.002
Syn65	2.50	0.90	9.30			
65 m	1.50 ± 0.55	1.03 ± 0.07	9.49 ± 0.16	0.67 ± 0.07	0.37 ± 0.07	0.022 ± 0.001

*Significant to the second digits only.
†The mean needle-probe conductivity values for BDP93 are 1.18 $Wm^{-1}K^{-1}$ between depths 28 and 58 m and 1.22 $Wm^{-1}K^{-1}$ between 58 and 88 m.
**The mean needle-probe conductivity values for BDP96 are 0.88 $Wm^{-1}K^{-1}$ between depths 35 and 65 m, and 0.90 $Wm^{-1}K^{-1}$ between 65 and 95 m.

DISCUSSION

A crucial question in any inverse modeling for parameter determination is the reliability of end results. The methods in common practice for estimating formation temperature tend to be simplistic because increasing the model sophistication may not be warranted in view of data quality or quantity. For example, the data used by Middleton (1979) are not numerous enough for our application. Based on an instantaneous line source, equation (3) works well for cooling a temperature probe that was inserted instantly into soft sediments (Hutchison and Owen, 1989; Lee et al., 2003) but may not be appropriate for thermal recovery after a borehole has endured a long period of mud circulation unless the observation times are far beyond the circulation time, as addressed earlier. Usually the zero circulation model of equation (2) is more appropriate at the bottom of the borehole than for the measurements made far above the bottom. At the very bottom, however, the axial (vertical) heat flux may become a factor to be reckoned. Equation (1) is thus preferred for mud circulation of long duration even though the circulation time is unknown or undefinable when the data from two holes are spliced together for BDP93. Additionally, the mud circulation was likely punctuated with disruption during drilling operations. The heat exchange between the circulating mud and the formation has never been steady, as assumed in our modeling. Despite these concerns, the diffusion processes will have smoothed the imprints of thermal irregularities if the records used are taken long after mud circulation ends.

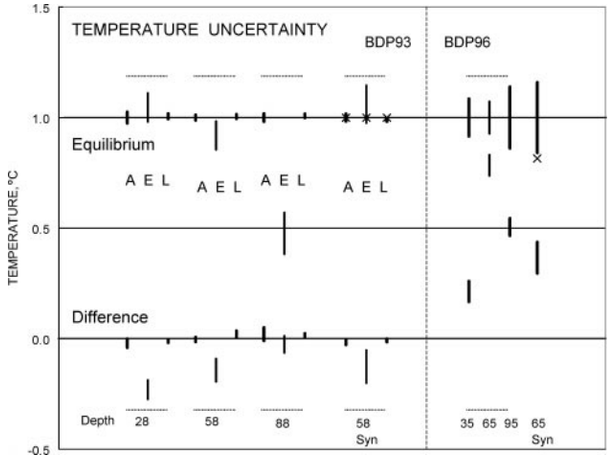

FIG. 4. Uncertainty in the determination of equilibrium formation temperature. Each pair of vertical bars represents the results for one data set. (E, L, and A stand for the early, late, and all-composite data segments, respectively.) Each upper bar for BDP93 denotes the mean formation temperature, plotted with reference to the value for A. All mean values for A at different depths are reset to 1°C for comparison. For BDP96, all mean formation temperature are also reset at 1°C. As a measure for model selection, each lower bar represents the mean value of the differences $\theta_{asy} - \theta_{equ}$. The length of each bar represents two standard deviations. The true values for synthetic data are marked by ×'s.

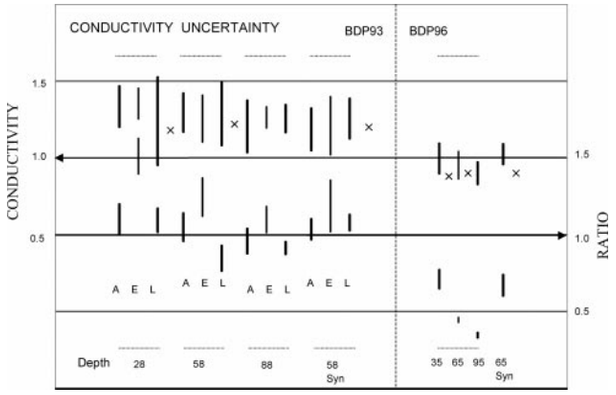

FIG. 5. Uncertainty in the determination of thermal conductivity. Each pair of vertical bars represents the results for one data set. Each upper bar centers at the mean conductivity, while the lower bar centers at the mean conductivity ratio of k_{asy}/k, which is a measure for model selection. The length of each bar represents two standard deviations. Each × symbol denotes the mean of conductivity values measured with the needle-probe method in cores between the indicated depth ranges, except that it represents the true value for the synthetic data. The conductivity is in units of $\mathrm{Wm^{-1}K^{-1}}$.

Formation temperature

The modeling results as measured by rms_2 (Table 2) appear acceptable because all rms are below a perceived error of 0.05°C except for BDP96-95m, which has an rms_2 of 0.06°C. The misfit distributions as represented by Figures 1 and 2 appear unbiased. Because the temperature was recorded to the nearest 0.01°C, the third decimal digit for the rms listing is insignificant. Nevertheless, the third decimals are retained to show small variations in rms_2 (<0.01° C). Frequently, the variations are too subtle to permit model selection by rms alone. We take the mean values as the final model parameters and append the standard deviations as the uncertainties.

At BDP93, the standard deviations of the equilibrium formation temperatures are less than 0.03°C for the late- and all-data models but reach 0.09°C for the early segments (Table 2, Figure 4). Similarly, the mean values are consistent (<0.01°C) with one another for the late- and all-data sets; but for the early segments, the mean equilibrium values deviate from those for the all- and late-data sets by 0.04°, 0.08°, and 0.5°C at depths of 28, 58, and 88 m, respectively. These patterns are also reflected in the distribution of the differences $\Delta\theta(=\theta_{asy} - \theta_{equ})$. The consistency suggests that θ_{equ} is well determined for late and all data. Greater uncertainty and discrepancy for the early-data segments seem to imply that the record lengths for the early segments are too short to allow a good estimate of θ_{asy}. This implication is contrary to the fact that the linear correlation coefficient for equation (1) is between −0.98 and −1.00 after some early data points are eliminated one by one (until at least five points remain) to establish a linear asymptotic relation.

The uncertainty in θ_{equ} and the discrepancy $\Delta\theta$ are relatively greater for BDP96 (Table 2, Figure 4). The $\Delta\theta$ (0.21°–0.78°C) are much greater than the data error of 0.05°C, and they are so large that the inclusion of S^{II} constraint cannot reduce the discrepancy to a satisfactory level. This failure is partly attributable to using a short shut-in time. Hence, the S^{II} constraint has not been implemented systematically in this study despite our original intention. The goodness of curve fitting in Figure 3 for BDP96 is visibly albeit slightly inferior to that in Figure 1 or 2 for BDP93. Based on the sizes of misfit rms and

the standard deviations of θ_{equ}, the accuracy in determining θ_{equ} for BDP96 is probably around 0.1°C. This translates into an error of ±0.03°C/m in the estimate of geothermal gradient or about 4% error at this site (the sensors are spaced 30 m apart in depth).

Conductivity

The uncertainties in thermal conductivity as measured by standard deviations are within ±10% except for 14% for all data at BDP93-88m (Table 2, Figure 5). Most ratios of k_{asy}/k are within ±0.1 from unity; notable exceptions appear at the early segment of BDP93-28m and at all three depths of BDP96. Good ratios support the notion that those model conductivity values are acceptable; poor ratios cast doubt on the results. Next, the assessment is made by comparing the model values with a set of independently measured conductivity values, although this optional, experimental comparison normally is not available for assessing inversion modeling in practice.

Thermal conductivity at BDP93 has been measured on drill cores. Duchkov and Kazantsev (1996) reported a conductivity value of 1.16 ± 0.17 $Wm^{-1}K^{-1}$ for 109 measurements in cores with a needle-probe method and a value of 1.76 ± 0.24 $Wm^{-1}K^{-1}$ for 553 measurements with a thermal comparator applied over the flat surface of lengthwise-sliced cores. The large discrepancy between the two sets of measured values (26% from their mean value of 1.46 $Wm^{-1}K^{-1}$) necessitated an independent study through inverse modeling of thermal recovery to properly determine terrestrial heat flow. Using a scheme similar to this one without using genetic algorithm to generate $\mathbf{p}^{guess}$, ignoring the conductivity ratio k_{asy}/k as a criterion, and keeping the modeler from knowing the two different sets of values, Duchkov et al. (2001) find a mean value of 1.26 $Wm^{-1}K^{-1}$ for the whole unshifted data by searching the set of $\mathbf{p}$ that gives the least misfit rms_2 through meticulously fine-tuning the input $\mathbf{p}^{guess}$. Since the model value is much closer to the needle-probe value, the needle-probe values were deemed preferable to the comparator values. A similar discrepancy between the results by the needle-probe and comparator methods has been reported elsewhere (e.g., the comparator value is greater than the needle-probe value by 13% on average; see Horai, 1981).

The needle-probe values (Duchkov et al., 2001) are listed in Table 2 for comparison with the results of the present modeling and plotted in Figure 5 for visual comparison. Relative to the needle-probe values, the model values for the early data are overestimated by 11% and 5% at depths between 28 and 58 m, and between 58 and 88 m at BDP93, respectively; the corresponding values for the late data are also overestimated, respectively, by 7% and 6%. For the composite data as a whole, the respective values are positively biased by 11% and 5%. For BDP96, the model conductivity values are overestimated relative to the needle-probe values by 11% and 3%, respectively, at depths between 35 and 65 m, and between 65 and 95 m. These comparisons indicate that model mean values, despite internal uncertainty of about 10%, are fairly reliable because a needle-probe value may have an uncertainty of 5% to 10% and because the quoted needle-probe values represent mean values for a long segment of cores while the model values represent a much narrower depth range of sediments around a temperature sensor.

The uncertainties in the estimates of heat capacity range from 12% to 40% for the results listed in Table 2. No independent measurement assesses the results, and the heat capacity must be viewed as undeterminable from the available data at this writing. Large uncertainties in heat capacity are associated with comparable uncertainties in the estimates of mud properties, initial mud temperature, and circulation time.

Synthetic data

Two sets of temperature–time data were computed with model parameters at BDP93-58m and BDP96-65m. Random errors up to ±0.03°C were imposed on the computed values to yield two sets of synthetic data, Syn58 and Syn65. The synthetic data were then modelled using the same procedures and parameter ranges for the corresponding sets of the real data. The genetic algorithm–inverse modeling procedures were run five times for each scenario.

Temperature.—The results (Table 2, Figure 4) for Syn58 indicate that both the formation temperatures θ_{equ} and discrepancies $\Delta\theta$ are determined within 0.01°C of the true values for late and all data. For the early segment, which exhibits the worst-case scenario for Syn58, the mean formation temperature errs by 0.06°C but the rms_2 of 0.033°C exceeds the data error by an insignificant 0.003°C. Like the case for the early-data segment of BDP93-58, the discrepancy $\Delta\theta$ of −0.13°C suggests that the record length may not be long enough to determine θ_{asy} from an asymptotic relation. For Syn65, the mean θ_{equ} errs by 0.19°C and the discrepancy $\Delta\theta$ reaches 0.37°C, even though an rms_2 of 0.022°C is still below the data error. These results suggest that the formation temperatures at BDP96 could err by similar magnitudes.

Figure 6 depicts the misfit distributions for the synthetic data. The parameters determined from the early segment are also used to predict the late temperatures, and vice versa. The data and model temperatures for the upper two sets of curves have been offset graphically to avoid overlapping. A solid curve represents a fitting based on a single set of model parameters, while a dashed curve represents the fitting obtained from the mean values for multiple genetic algorithm–inverse modeling runs. Note that models derived from the early data yield systematic misfits in extrapolation to late data (middle curves); the dashed curve extrapolates slightly better than the solid curve. For models based on late data (upper curves), the extrapolation shown by the dashed curve performs much better. The fact that the models of multiple genetic algorithm–inverse modeling runs can outperform the single-run models supports our practice of using the averages as the model parameter values.

Also depicted in Figure 6 is the fitting for Syn65. This plot provides a perspective of thermal recovery at the two Lake Baikal sites. The relatively greater slope for Syn65 over the identical postdrilling period indicates that the thermal conductivity at BDP96 should be less than that at BDP93, as demonstrated by the genetic algorithm–inverse modeling results (Table 2). Modeling the synthetic data indicates greater uncertainties are expected in the parameter estimates for BDP96.

Thermal properties.—For Syn58, the conductivity generated from the early data is essentially identical to the true value, but

a conductivity ratio k_{asy}/k of 1.19 suggests that the asymptotic relation is not yet established for the early segment of data. Both the late segment and the all composite data yield acceptable conductivity (<5%) and ratio (± 5%). For Syn65, the conductivity is underestimated by 14% (worse than that for the corresponding real data if the needle-probe value is true) and the conductivity ratio is unacceptably small.

Errors in estimating the heat capacity of sediments are unacceptably large except for the early segment at Syn58, which also yields the least error in the estimate of heat capacity for the mud (not listed). The late segment has the greatest error in the estimates of conductivity for the mud. The errors in the estimates of initial mud temperatures range from 0.2° to 0.3°C, being greatest for the late segment as expected.

CONCLUSION

We have used a genetic algorithm and quasi-linear inversion modeling to determine equilibrium temperature and thermal conductivity from the thermal recovery data. We have also used multiple genetic algorithm–inverse modeling runs to establish uncertainty, misfit rms, discrepancy $\Delta\theta$, and conductivity ratio k_{asy}/k for assessing the reliability of parameter determinations. The test data are highly noisy and require ad hoc manipulation of data sets. The conclusions, favorable or unfavorable, should be viewed with some reservation.

Despite the nonideal data at BDP93, the modeled equilibrium temperatures θ_{equ} are compatible with the results θ_{asy} obtained by a commonly used method for estimating equilibrium temperature [equation (1)]. The discrepancy increases with decreasing depth (Table 2) for the early data segments, suggesting that the expected increase in t_D/t or decline in $t - t_D$ degrades the applicability of the analytic solution. This upward deterioration trend is shared by the conductivity ratio k_{asy}/k. Generally the deviations of the model conductivity values from the needle-probe values also increase with decreasing depth, but there is no clear pattern of deviations as related to the early or late data. The trend of deviations could be caused by the greater uncertainty in t_D itself at shallower depth. The θ_{equ} values for the early, late, and all composite data at each depth are fairly consistent (around the estimated data error of 0.05°C) except for the early segment BDP93-88 m, where it is lower by 0.5°C for unknown reasons. The results for the synthetic data Syn58 substantiate the feasibility of using our method.

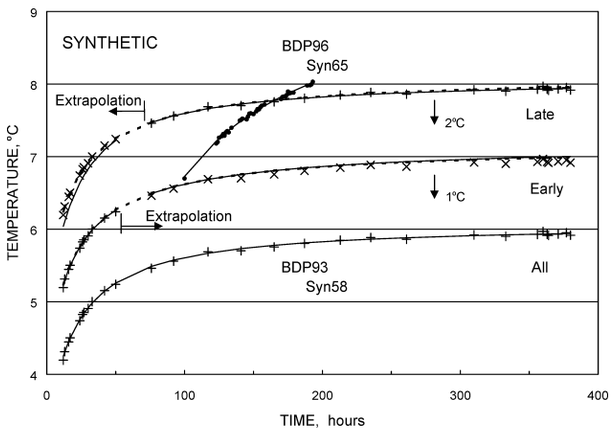

FIG. 6. Models of synthetic thermal recoveries, Syn58 and Syn65. The curves associated with ×-marked data represent extrapolations (or predictions) that are computed with model parameters obtained from data marked with +'s. Each solid model curve is based on one genetic algorithm–inverse modeling run, while a dashed model curve is based on multiple runs. The early and late data sets have been offset by 1° and 2°C, respectively, for plotting.

For BDP96, the discrepancy and conductivity ratio as two measures for assessing the modeling results fail. However, the closeness of the model conductivity values to the needle-probe values (Table 2) suggests that if the modeling results are wrong, the error is very likely much less than the error incurred when the analytic solution is used alone. Acceptable but imperfect results are generated for Syn65. The imperfection occurs because the data-time coverage is narrow and the overall postdrilling time is short (Figure 6).

We estimated the average rate of heat exchange Q between mud circulation and the formation and used it to obtain an asymptotic conductivity k_{asy} from equation (1). The ratio k_{asy}/k is expected to be 1 despite the fact that equation (1) is formulated for a steady heat exchange rate and our recovery model is based on a steady circulating mud temperature. This oneness is essentially achieved for a data set that includes both early and late data; but if the data are available only for a small time span, the oneness may not be achievable. In this case, it does not necessarily imply a failure in our method, as demonstrated by the modeling for BPD93 and Syn65.

The genetic algorithm is a biased stochastic process for solving a differential equation, but the results of genetic algorithm may not yield randomly distributed misfits. The inverse model modifies the genetic algorithm-generated parameter values to yield randomly distributed misfits and reduce the rms further. However, in some data-dependent cases the inverse model is unable to modify significantly the genetic algorithm-generated parameter values (to the third significant digit). Inverse modeling crashes frequently but rarely if $\mathbf{p}^{guess}$ is provided by the genetic algorithm. Through the genetic algorithm, many sets of parameters can be generated; most of their misfit rms are similarly low and on par with the data error, but individual parameters can vary significantly (>10%). Hence, it is advisable to run GA-IM 5–10 times and take the arithmetic means as the representative values, as practiced here. If justified, the parameters associated with an outlier result can be excluded from the averaging or the averaging can be weighted according to the size of their rms (not practiced here).

Overall, the results of our test cases for inverse modeling of thermal recovery are not entirely satisfactory. The constraint of S^{II} [equation (13)] has not been systematically exercised because (1) the discrepancy $\Delta\theta(=\theta_{asy}-\theta_{equ})$ obtained without this constraint is already on par with the data error; (2) if the $\Delta\theta$ is significantly large, imposing the constraint still cannot reduce $\Delta\theta$ to a satisfactory level (<0.05°C for our noisy test data); and (3) the postdrilling time $t - t_D$ is too short to warrant the use of equation (1), especially for the early data segments or measurements at shallow borehole depths. Our test data happen to represent these two bipolar situations, mainly a consequence of different time-sampling spans or durations of data coverage as substantiated through modeling the synthetic data. We anticipate that data of better quality and coverage will produce much better results, as demonstrated in a recent study on cooling recovery (Lee et al., 2003) which, unlike the

present model of finite mud circulation, is based on an instant heating model and on a constraint derived from equation (3) rather than equation (1).

ACKNOWLEDGMENTS

We appreciate the comments made by two anonymous reviewers.

REFERENCES

Bathe, K. J., and Wilson, E. L., 1976, Numerical methods in finite element analysis: Prentice-Hall, Inc.

Bullard, E. C., 1947, The time necessary for a borehole to attain temperature equilibrium: Monthly Notices of Roy. Astr. Soc., **5**, 127–130.

Cao, S., Lerche, I., and Hermanrud, C., 1988, Formation temperature estimation by inversion of borehole measurements: Part II—Effects of fluid penetration on bottom-hole temperature recovery: Geophysics, **53**, 1347–1354.

Carslaw, H. S., and Jaeger, J. C., 1959, Conduction of heat in solids: Oxford University Press.

Deming, D., 1989, Application of bottom-hole temperature corrections in geothermal studies: Geothermics, **18**, 775–786.

Deming, D., and Chapman, D. S., 1988, Inversion of bottom-hole temperature data, the Pineview field, Utah–Wyoming thrust belt: Geophysics, **49**, 453–466.

Drury, M. J., 1984, On a possible source of error in extracting equilibrium formation temperatures from borehole BHT data: Geothermics, **13**, 175–180.

Duchkov, A. D., 1991, Review of Siberian heat flow data. *in* Cermak, V., and Rybach, L., Eds., Terrestrial heat flow and lithosphere structure: Springer-Verlag, Berlin, 426–443.

Duchkov, A. D., and Kazantsev, S. A., 1996, Temperature measurement in the first underwater boreholes in Lake Baikal: Russian Geol. Geophys., **37**, 94–102.

Duchkov, A. D., Lee, T.-C., and Morozov, S. G., 2001, Thermal properties of bottom sediments of Lake Baikal: Russian Geol. Geophys., **42**, 288–296.

Forster, A., and Merriam, D. F., 1999, Problems and potential of industrial temperature data from a cratonic basin environment, *in* Forster, A., and Merriam, D. F., Eds., Geothermics in basin analysis: Kluwer Academic/Plenum Publishers, 35–59.

Horai, K., 1981., Thermal conductivity of sediments and igneous rocks recovered during Deep Sea Drilling Project Leg 60, *in* Hussong, D. M., and Uyeda, S., Eds., Initial reports, Deep Sea Drilling Projects, **60**, 807–834.

Hutchison, I., and Owen, T., 1989, A microprocessor heat flow probe, *in* Wright, J. A., and Louden, K. E., Eds., Handbook of seafloor heat flow: CRC Press, 71–90.

Jones, F. W., Rahman, M., Leblanc, Y., 1984, A three-dimensional numerical bottom-hole temperature stabilization model: Geophys. Prosp., **32**, 18–36.

Kalinin, A. N., Sokolova, L. S., Duchkov, A. D., and Chrepanov, V. Y., 1983, Investigation of a thermal comparator for measuring the thermal conductivity of rocks: Soviet Geol. Geophys., **24**, 109–114.

Lachenbruch, A. H., and Brewer, M. C., 1959, Dissipation of temperature effect of drilling a well in arctic Alaska: Bull. U.S. Geol. Surv., **1083-C**, 73–109.

Leblanc, Y., Pascoe, L. J., and Jones, F. W., 1981, The temperature stabilization of a borehole: Geophysics, **46**, 1301–1303.

Lee, C.-Y., Ma, L., and Antonsson, E. K., 2001, Evolutionary and adaptive synthesis methods, *in* Antonsson, E. K., and Cagan, J., Eds., Formal engineering design synthesis: Cambridge Univ. Press, 270–320.

Lee, T.-C., 1982, Estimation of formation temperature and thermal property from dissipation of heat generated by drilling: Geophysics, **47**, 1577–1584.

——— 1989, Thermal conductivity measured with a line source between two dissimilar media equals their mean conductivity: J. Geophys. Res., **94**, 12443–12447.

——— 1999, Applied mathematics in hydrogeology: Lewis Publishers.

Lee, T.-C., and von Herzen, R. P., 1994, In-situ determination of thermal properties in sediments using a friction-generated probe source: J. Geophys. Res., **99**, 12121–12132.

Lee, T.-C., Duchkov, A. D., and Morozov, S. G., 2003, Determination of thermal conductivity and formation temperature from cooling history of friction-heated probes: Geophys. J. Internat., **152**, 433–442.

Lee, T.-C., Perina, T., and Lee, C.-Y., 2002, Validation of aquifer parameter determination by extrapolation fitting and treating thickness as an unknown: J. Hydrol., **265**, 15–33.

Luheshi, M. N., 1983, Estimation of formation temperature from borehole measurements: Geophys. J. Roy. Astr. Soc., **74**, 746–776.

Majorowicz, J. A., and Jessop, A. M., 1981, Regional heat flow patterns in the western Canadian sedimentary basin: Tectonophysics, **74**, 209–238.

Majorowicz, J. A., Garven, G., Jessop, A., and Jessop, C., 1999, Present heat flow along a profile across the western Canada sedimentary basin, the extent of hydrodynamic influence, *in* Forster, A., and Merriam, D. F., Eds., Geothermics in basin analysis: Kluwer Academic/Plenum Publishers, 61–79.

Middleton, M. F., 1979, A model for bottom-hole temperature stabilization: Geophysics, **44**, 1458–1462.

Reiter, M., Eagleston, R. E., Broadwell, B. R., and Miner, J., 1986, Estimates of terrestrial heat flow from deep petroleum tests along the Rio Grande rift in central and southern New Mexico: J. Geophys. Res., **91**, 6225–6245.

Shen, P. Y., and Beck, A. E., 1986, Stabilization of bottom hole temperature with finite circulation time and fluid flow: Geophys. J. Roy. Astr. Soc., **86**, 63–90.

Tarantola, A., 1987, Inverse problem theory: Elsevier, Science Publ. Co. Inc.

Towend, J., 1997, Estimates of conductive heat flow through bottom-simulating reflectors on the Hikurangi and southwest Fiordland continental margins, New Zealand: Marine Geol., **141**, 209–220.

——— 1999, Heat flow through the west coast, South Island, New Zealand: New Zealand J. Geol. Geophys., **42**, 21–31.

von Herzen, R. P., and Maxwell, A. E., 1959. The measurement of thermal conductivity of deep-sea sediments by a needle probe method: J. Geophys. Res., **64**, 1557–1563.